The aerodynamics of the beautiful game

John W. M. Bush

Department of Mathematics, MIT

Abstract

We consider the aerodynamics of football, specifically, the interaction between a ball in flight and the ambient air. Doing so allows one to account for the characteristic range and trajectories of balls in flight, as well as their anomalous deflections as may be induced by striking the ball either with or without spin. The dynamics of viscous boundary layers is briefly reviewed, its critical importance on the ball trajectories highlighted. The Magnus effect responsible for the anomalous curvature of spinning balls is seen to depend critically on the surface roughness of the ball, the sign of the Magnus force reversing for smooth balls. The origins of the fluttering of balls struck with nearly no spin is also discussed. Particular attention is given to categorizing and providing aerodynamic rationale for the various free kick styles.

1 Introduction

Fluid dynamics is the science that allows us to rationalize the flow of fluids, either liquids or gases, and so understand a vast array of everyday phenomena (Batchelor 1967, Acheson 1990). Aerodynamics is the subset of fluid dynamics dealing with the flow of air. In addition to informing the design of airplanes and providing the rationale for the flight of birds and insects, it provides the basis for understanding the trajectory of sports balls in flight. A comprehensive treatment of this more general subject, sports ball aerodynamics, can be found in Daish (1972), Mehta (1985, 2009) and Mehta & Pallis (2001), while the aerodynamics of specific sports, including golf (Erlichson 1983), cricket (Mehta *et al.* 1983, Mehta 2005), tennis (Mehta *et al.* 2008), baseball (Watts & Sawyer 1975, Frolich 1984, Adair 2002, Nathan 2008) and american football (Gay 2004) have been treated elsewhere. We here focus specifically on the dynamics of soccer, or as most of the world knows it, football. The bulk of the research reported here is not original. While it does draw in part upon recent studies of the aerodynamics of football (Asai *et al.* 2007, Hong *et al.* 2010, Dupeux *et al.* 2010, Hong & Asai 2011, Goff 2010, Goff & Carré 2010, 2012), it is more a personal than a scholarly account, an idiosynchratic pedagogical review of the relevant aerodynamics integrated with my experience as a soccer player.

Ballistics is the study of objects flying through the air, one that has received considerable attention owing to its military applications. We begin by considering the simplest possible

theoretical description of a football in flight, that of a sphere of mass m flying through a vacuum, in which there is no aerodynamic influence on the motion, a classic high school physics problem. The trajectory of the ball $\mathbf{x}(t) = (x(t), z(t))$ can be simply expressed through Newton's first law:

$$m\ddot{\mathbf{x}} = -m\mathbf{g}, \tag{1}$$

where $\mathbf{g} = -g\ \hat{\mathbf{z}}$ is the acceleration due to gravity. This equation may be solved subject to the initial conditions $(x, y) = (0, 0)$ and $(\dot{x}, \dot{z}) = (U\cos\theta, U\sin\theta)$, where θ is the initial take-off angle. Doing so yields the trajectory $(x(t), z(t)) = (U\cos\theta t,\ U\sin\theta\ t - \frac{1}{2}gt^2)$. As indicated by the uppermost curve in Figure 1, this trajectory is symmetric, with the second half of its trajectory being the mirror image of its first. Setting $z = 0$ indicates that the time of flight is $t_f = 2U\sin\theta/g$. The range of the ball is thus $x(t_f) = U^2\sin 2\theta/g$, and achieves a maximum of U^2/g with a take-off angle of $\theta = 45°$.

The characteristic release speed of a well struck goal kick is approximately 30 m/s. Kicking a soccer ball at this speed at the optimal angle of 45° indicates a maximum range of 120m, which is nearly twice that observed. Moreover, casual observation indicates that the average goal kick violates the symmetry of the predicted trajectory, with the ball falling more steeply than it climbs. Experienced players know that the range of a goal kick may be extended by imparting backspin to the ball, and that 45° is not necessarily the optimal launch angle. Finally, it is common for long kicks to stray from a vertical plane. None of these features can be rationalized without considering the influence of the ambient air on the flight of the ball.

Quite generally, an object moving at a speed U through a fluid experiences resistance that depends on the fluid properties, specifically its density ρ and dynamic viscosity μ (or alternatively, the kinematic viscosity, $\nu = \mu/\rho$). This resistance in general has two components, viscous drag and pressure (or 'form') drag. Flow of a fluid past a solid exerts a tangential stress (force per unit area) of $\mu U/a$, where U/a is the local shear on the solid's boundary. Consequently, we anticipate that the characteristic viscous drag on a sphere of radius a will be obtained by multiplying this characteristic viscous stress by the surface area of the sphere, $4\pi a^2$, thus yielding a viscous drag proportional to $D_v \sim \mu U \pi a$. The pressure drag arises from a pressure difference between the front and back of the ball. The magnitude of this pressure difference in general depends on the details of the flow, but typically scales as ρU^2. The resulting pressure drag is thus obtained by multiplying this pressure difference by the exposed area of the sphere, and so is proportional to $D_p \sim \rho\pi a^2 U^2$. The relative magnitudes of these characteristic pressure and viscous drags is given by the Reynolds number:

$$Re = \frac{\text{PRESSURE DRAG}}{\text{VISCOUS DRAG}} = \frac{Ua}{\nu}. \tag{2}$$

The Reynolds number characterizing the flight of a number of sports balls is included in Figure 2. Note that the Reynolds number is high for all sports balls, and the largest for footballs owing to the relatively large speed and ball size.

The pressure drag is thus dominant for most sports balls, including footballs, and a good approximation for the drag is a force opposing motion with magnitude $C_D \rho U^2 \pi a^2/2$, where a is the ball radius, ρ is the air density, and U is the ball speed. The drag coefficient C_D is in general a function of both Re and surface roughness, but is an order 1 constant at the high Re appropriate for ball sports. The empirical dependence of C_D on Re has been well characterized for a smooth ball, for which $C_D \sim 0.4$ for $10^3 < Re < 2 \times 10^5$ (Smith *et al.*, 1999). As Re is further increased, C_D decreases dramatically to a value of approximately 0.1 before recovering to a value of approximately 0.4 for $Re > 10^7$. This precipitous drop in C_D, termed the drag crisis, plays a critical role in many ball sports (Mehta 1985, Mehta & Pallis 2001), including football. The critical Reynolds number Re_c at which the drag crisis arises varies from sport to sport, as it is strongly influenced by the ball's surface roughness. For example, the dimples on a golf ball prompts the drag crisis at $Re_c = 5 \times 10^4$, the paneling on a football at $Re_c = 10^5$, the corresponding speed being roughly 15 m/s.

Incorporating aerodynamic drag leads to an improved equation for the trajectory of a ball in flight. Denoting the position of the ball's center by $\mathbf{x}$ and its velocity by $\dot{\mathbf{x}} = \mathbf{U} = U\hat{\mathbf{s}}$, we augment (1) to deduce:

$$m\ddot{\mathbf{x}} \;=\; m\mathbf{g} - C_D \; \pi a^2 \rho \; |\dot{\mathbf{x}}|^2/2 \; \hat{\mathbf{s}} \quad , \tag{3}$$

where we again stress that the drag coefficient C_D depends in general on both $Re = Ua/\nu$ and the sphere's surface roughness. Nondimensionalizing (3) on the basis of the a length-scale corresponding to the ball radius a, a velocity scale U_0 and a timescale a/U_0 yields a dimensionless trajectory equation for the dimensionless ball position $\mathbf{X} = \mathbf{x}/a$:

$$A \; \ddot{\mathbf{X}} \;=\; -\hat{\mathbf{z}} \;-\; \frac{C_D}{2B} \; |\dot{\mathbf{X}}|^2 \; \hat{\mathbf{s}} \quad . \tag{4}$$

Two dimensionless groups appear. We refer to the first, $A = U_0^2/(ga)$, as the range parameter, which indicates the relative magnitudes of the maximum range of the ball in vacuo, U_0^2/g, and the ball radius a. We refer to the second as the coefficient of ballistic performance:

$$B = \frac{\text{WEIGHT}}{\text{AIR DRAG}} = \frac{mg}{\pi \rho a^2 U_0^2}, \tag{5}$$

which indicates the relative magnitudes of the ball's weight and the aerodynamic drag force at launch. The ballistic performance indicates how important aerodynamic forces are on the trajectory of a ball in flight. B values for a number of common ball games are listed in Table 1. Note that aerodynamic forces are most important for light balls: it is thus that one can throw a golf ball much farther than a ping pong ball.

Figure 1a indicates the trajectories computed from (4) using the same release speed ($U = 32$ m/s, corresponding to $A = 910$) and launch angle, 45°, for balls with different B values. For high B, the trajectory is virtually unaffected by aerodynamic effects, and so follows a nearly parabolic trajectory. Such is the case for the shot put. Conversely, for small B values, aerodynamic forces lead to a rapid deceleration of the ball, and a striking

asymmetry in the ascending and descending portions of the trajectory; specifically, the ball speed decreases rapidly, and falls relatively steeply from the apex of its trajectory. One can thus rationalize the asymmetry of goal kicks in football, which reflects the influence of aerodynamic drag on the trajectory. Incorporating air drag reduces B from ∞ to 0.1 for the case of a football in flight, and so reduces the predicted range of goal kicks from 120m to 60m, which is more consistent with observation. Figure 1b indicates the influence of aerodynamic drag on the flight of a football struck at 25m/s. Once again, the range is reduced by the incorporation of air drag. The lower curve indicates the influence of the drag crisis (to be discussed in §3), which further reduces the range, and heightens the asymmetry of the trajectory. As we shall see, consideration of the influence of air on the football not only allows us to improve our estimate for the range of a goal kick, but to rationalize the motion of the ball out of the vertical plane, the anomalous curvature of spinning and non-spinning balls in flight.

2 The equations of fluid motion

While we have already demonstrated the importance of air drag in rationalizing the range of a football, it is important to understand its origins if we are to come to grips with more subtle aerodynamic effects such as the Magnus and reverse Magnus effects. Just as Newton's Laws describe the motion of discrete particles, Navier-Stokes equations describe the motion of an incompressible fluid of constant density ρ and viscosity $\mu = \rho\nu$ in the presence of a gravitational field $\mathbf{g}$. The velocity $\mathbf{u}$ and pressure p fields within a fluid evolve according to

$$\rho\left(\frac{\partial \mathbf{u}}{\partial t} \; + \; \mathbf{u}\cdot\nabla\mathbf{u}\right) = -\nabla p_d \; + \; \rho\nu\nabla^2\mathbf{u} \quad , \quad \nabla\cdot\mathbf{u} \; = \; 0 \quad . \tag{6}$$

where $p_d = p - \rho g z$ is the dynamic pressure (Acheson 1990). The fluid momentum may change as a result of inertial forces, dynamic pressure gradients within the fluid, and viscous stresses, which act everywhere to suppress velocity gradients and so resist motion. Equation (6) is a formidable equation that can only be solved exactly for some very simple flows, the high Re flow around a football not being one of them. We thus proceed by assessing the relative magnitudes of the terms in (6), with hopes that some of them will be negligibly small.

Consider a sphere of radius a moving through a fluid at speed U. We define dimensionless (primed) quantities in terms of dimensional ones:

$$\mathbf{u}' = \mathbf{u}/U \quad , \quad \mathbf{x}' = \mathbf{x}/a \quad , \quad t' = t\;U/a \quad , \quad p' = p/(\rho U^2) \quad . \tag{7}$$

Rewriting (6) in terms of these dimensionless variables and dropping primes yields

$$\frac{\partial \mathbf{u}}{\partial t} \; + \; \mathbf{u}\cdot\nabla\mathbf{u} = -\nabla p_d \; + \; \frac{1}{Re}\,\nabla^2\mathbf{u} \quad , \tag{8}$$

where we again see the emergence of the Reynolds number $Re = Ua/\nu$. We have seen previously that the characteristic Re of a football in flight is in excess of 10^4, and so might feel justified in neglecting the final term in (6), that represents the viscous stresses within the fluid. We would thus obtain the Euler equations that describe the flow of inviscid fluids:

$$\frac{\partial \mathbf{u}}{\partial t} \; + \; \mathbf{u} \cdot \nabla \mathbf{u} = -\nabla p_d \quad . \tag{9}$$

In the limit of steady flow, as one might expect to arise for a ball flying through the air at uniform speed, (8) may be expressed as

$$\nabla (p + \frac{1}{2} \rho u^2) = 0 \quad : \tag{10}$$

along a streamline of the flow, $p + \frac{1}{2}\rho u^2 = constant$, a result known as Bernoulli's Theorem. If the flow speed increases along a streamline, the pressure necessarily decreases, and vice versa.

D'Alembert's Paradox is the inference that the drag on a body moving steadily through an inviscid fluid must vanish (Batchelor, 1967). This may be seen simply for the case of a spherical object: since the streamlines computed for inviscid flow around a sphere are fore-aft symmetric, so too must be the pressure distribution. As the drag on the sphere in the high Re limit is deduced by integrating the fluid pressure over the sphere, this calculation indicates zero drag. We have already stated that the aerodynamic drag on balls in flight is non-zero, of order $\pi a^2 \rho U^2$, so what have we missed?

3 Boundary layers

The complete neglect of viscous effects is an untenable approximation, even in the limit of exceedingly large Re, as it gives rise to a number of conceptual difficulties, including D'Alembert's Paradox. While viscosity is negligible on the scale of the flow around the ball, it becomes significant in a thin boundary layer of thickness δ adjoining the ball. Within the boundary layer, viscous forces $\mu \nabla^2 \mathbf{u} \sim \mu U/\delta^2$ are comparable to inertial forces $\mathbf{u} \cdot \nabla \mathbf{u} \sim U^2/a$, the balance of which indicates a boundary layer thickness $\delta \sim aRe^{-1/2}$. As evident in Figure 2, Reynolds numbers are high in all ball sports, so the corresponding boundary layers are thin. In football, for example, the characteristic boundary layer thickness is $\delta \sim 0.1$mm.

How is it that incorporating viscosity can give rise to a drag force of order $\rho U^2 \pi a^2$ that does not depend explicitly on viscosity? The influence of the viscous boundary layer is two-fold. First, it ensures that there will always be some non-zero drag on an object through the influence of viscous stress. For high Re flow past an object, the viscous drag per unit area generated within its boundary layer, or skin friction, scales as $\mu U/\delta$. Thus, the characteristic viscous drag acting on a ball in flight will scale as $\mu U \pi a^2/\delta$. For the Reynolds numbers appropriate for most sports balls (Figure 2), this viscous contribution to the total drag is

negligible. The dominant effect of the viscous boundary layer is to initiate boundary layer separation, thus breaking the symmetry of the flow and giving rise to a non-zero pressure drag of order $\rho U^2 \pi a^2$.

Flow past a smooth, rigid sphere is a canonical problem that has been studied exhaustively both experimentally and theoretically (Shapiro 1961, Smith *et al.* 1999). At low Re, the flow is dominated by viscous stresses, and the streamlines are symmetric fore and aft of the sphere (Figure 3a). The drag on the sphere, $D = 6\pi\mu U a$, increases linearly with both the flow speed U and the fluid viscosity. The flow remains viscously dominated until $Re \sim 1$, when inertial drag associated with a fore-to-aft pressure drop becomes significant. At $Re = 10$, a laminar ring vortex is established downstream of the sphere (Figure 3b). For $Re > 100$, this vortex becomes unstable, and the resulting time-variation in the downstream pressure field gives rise to a lateral force on the ball (Figure 3c). In a certain regime, the vortex peals off the back of the ball like a helix; consequently, the sphere proceeds in a spiraling fashion. This transition from rectilinear to helical motion may be observed in fireworks, and also in your local bar. For similar reasons, champagne bubbles rise in straight lines (Liger-Belair, 2004), while their relatively high-Re counterparts in a beer glass spiral as they rise.

As Re is further increased, the flow in the wake becomes progressively more complex until achieving a turbulent state (Figure 3d). Then, the pressure in the wake is effectively uniform, and determined by the pressure in the free stream at the point of separation of the wake. As Re increases, this point of separation generally moves upstream towards the equator of the sphere. Thus, the pressure in the wake decreases, while the area of the wake increases, the net effect being a drag that increases monotonically with Re. Finally, when the separation line reaches the equator, the drag on the sphere achieves its maximum, as the pressure drop fore-and-aft is maximum, as is the area over which the anomalous pressure low in the wake acts (Figure 3e). In this configuration, it is simple to make a reasonable estimate for the fore-aft pressure drop, which should correspond to the pressure drop along the streamline passing from the upstream stagnation point to the equator, $\rho U^2 a^2/2$, according to Bernoulli's Theorem. Further increasing Re beyond a critical value of 2×10^5 on a smooth ball prompts the drag crisis, at which the drag drops drastically, typically by a factor of 3 (Figure 3f). Here, the boundary layer on the leading face of the sphere becomes turbulent, the effect being to displace the point of boundary layer separation downstream, and so reduce the drag. This delay in the boundary layer separation may be understood as being due to the boundary layer turbulence mixing high-momentum fluid down from the laminar external flow (Shapiro 1961).

The sensitivity of the aerodynamic force to the drag crisis plays a critical roll in a number of ball sports. The progression detailed in Figure 3 is that observed on a smooth ball; however, the progression is qualitatively similar on rough balls. Most sports balls have some roughness elements, either fuzz in the case of tennis balls (Mehta *et al.* 2008), stitches in the case of cricket (Mehta *et al.* 1983, Mehta 2005) and baseballs (Nathan 2008), or dimples in the case of golf balls (Erlichson 1983). For all such balls, the roughness serves to

encourage turbulent rather than laminar boundary layers, so that the drag crisis is achieved at lower speeds, and the drag greatly decreased. As previously noted, the drag crisis arises at $Re \sim 2 \times 10^5$ on smooth ball, $Re \sim 10^5$ for footballs and $Re = 3 \times 10^4$ for golf balls, whose range is thus doubled by the presence of the dimples. Controlled orientation of the stitches on baseball and cricket balls gives rise to anomalous lateral or vertical forces owing to the asymmetry of the boundary separation on the ball's surface, an effect exploited by pitchers and bowlers, respectively (Mehta and Pallis 2001).

The stitching of footballs ensures that, at the peak speeds relevant for shooting, the boundary layer is typically turbulent. However, as the ball decelerates in response to aerodynamic drag, its Re likewise decreases, ultimately reaching the critical value of 10^5 at a speed of $U \sim 15$m/s. It then crosses the drag crisis threshold from above, at which point its boundary layers transition from turbulent to laminar. Consequently, the drag increases by a factor of approximately 3, and the ball decelerates dramatically. On a goal kick or a free kick, this drag crisis typically arises during the descent phase; thus, it will amplify the asymmetry of the trajectories apparent in Figure 1a. The influence of the drag crisis on a ball struck at $U_0 = 25$ m/s is illustrated in Figure 1b. As we shall see in §4, the drag crisis will have an even more striking effect on spinning walls in flight.

Finally, we note that the progression detailed in Figure 3 of flow past a sphere is qualitatively different for streamlined bodies. If a body is shaped like a modern airfoil or, for that matter, like a trout, one can avoid boundary layer separation entirely. In this case, the drag is prescribed entirely by the applied viscous stress or skin friction. As the Reynolds number increases, the boundary layer thickness scales like $\delta \sim aRe^{-1/2}$, and the skin friction like $\tau_s \sim \mu U/\delta$. The ratio of the skin friction drag τa^2 to the form drag associated with the fore-aft pressure drop across a bluff body, $\rho U^2 a^2$, is thus given by $Re^{-1/2}$. At the high Re appropriate for many modern sports, including ski racing and cycling, one can thus readily see the tremendous advantage of streamlining, now the basis for an enormous sports industry.

4 The effect of spin

4.1 The Magnus effect

The Magnus Effect is the tendency of a spinning, translating ball to be deflected laterally, that is, in a direction perpendicular to both its spin axis and its direction of motion. For example, if spin is imparted such that the angular velocity vector has a vertical component, the ball will be deflected out of the vertical plane depicted in Figure 1 by the Magnus force. The role of the Magnus effect on the flight of tennis balls was noted by Newton (1672), then again by Lord Rayleigh (1877), who remarked "...a rapidly rotating ball moving through the air will often deviate considerably from the vertical plane." The influence of spin on the flight of cannon balls was examined in 1742 by the British artillery officer Robins (1805).

The effect takes its name from Professor Heinrich Gustav Magnus (1853), a physicist and chemist at the University of Berlin, who measured the lateral force on cylinders rotating in an air current. The first theoretical description of the effect was presented by Lord Rayleigh, whose theory predicted that the lift is proportional to the product of the speeds of rotation and translation. However, it was not until the theory of boundary layers, developed by Ludwig Prandtl (1904; see also Schlichting 1955, Anderson 2005), that the subtlety of the effect could be fully appreciated.

The Magnus effect has received considerable attention owing to its importance in ballistics. When cylindrical shells are fired from guns or cannons, they are often spin stabilized: rotational angular momentum imparted by fluting of the rifle shaft keeps the shells from tumbling in flight, thus maximizing their speed and range. When fired into a cross wind, or fired from a moving ship or plane, this spin interacts with the translation of the shell to generate an anomalous lift force, that may cause the shell to miss its target. Ballistics experts and snipers are thus well aware of the Magnus effect and how to correct for it. The Magnus effect has inspired a number of inventions, some of them unlikely. The Flettner rotor is a sailboat whose sail is replaced by a rotating cylinder (Figure 4a). The motion of the cylinder is driven by a generator, and interacts with the wind to drive the boat forward via Magnus forces. The Flettner rotor boat has successfully circumnavigated the globe, and new styles of Magnus sailboats are currently being explored owing to their energy efficiency. More surprising still is the Magnus airplane, for which lift is generated by flow over wings comprised of rotating cylinders (Figure 4b). While the lift forces so generated may be higher than those generated on conventional airfoil wings, the relatively large drag induced by their cylindrical form make this design impractical.

The Magnus effect is also exploited in a number of Nature's designs. Many seed pods, including maple keys, are shaped such that they tumble as they fall (Figure 5a; Vogel 2003). The coupling of the resulting rotational and translational motions can give rise to a Magnus lift force that considerably extends the range of these seeds pods, thus giving them an evolutionary advantage. It has also been claimed that the range of the box mite, that rotates when it leaps, is increased by the Magnus effect (Figure 5b; Wauthy et al.1998).

For a ball in flight with velocity $\dot{\mathbf{x}} = \mathbf{U} = U\hat{\mathbf{s}}$ that is also spinning with angular velocity $\mathbf{\Omega}$, in addition to drag, there is thus a lift force in a direction perpendicular to both $\mathbf{\Omega}$ and $\mathbf{U}$. This so-called Magnus force takes the form $\mathbf{F_M} = C_L \pi \rho a^3 \, \mathbf{\Omega} \wedge \mathbf{U}$. We can thus augment (3) to deduce the trajectory equation for a translating, spinning ball:

$$m\ddot{\mathbf{x}} \;=\; m\mathbf{g} - C_D \, \pi a^2 \rho \, U^2 \, \hat{\mathbf{s}} \;+\; \mathbf{C_L} \, \pi \mathbf{a^3} \rho \, \mathbf{\Omega} \wedge \mathbf{U} \quad . \tag{11}$$

The lift coefficient C_L, like the drag coefficient C_D, is an order one constant that depends on both the Re and the sphere's surface roughness; furthermore, C_L depends on the spin parameter $S = \Omega a/U$, that prescribes the relative magnitudes of the the ball's rotational and translational speeds. We note that in all sports, one may safely assume that $0 < S < 1$, as is evident in the estimates presented in Figure 2. As we shall see in what follows, the

dependence of C_L on Re, S and the surface roughness is quite dramatic; for example, altering a ball's surface roughness can change the sign of C_L.

Bernoulli's Theorem provides a simple but ultimately unsatisfactory rationale for the anomalous trajectories of spinning balls in flight. Imagine a ball flying through the air with pure backspin or 'slice', so that its rotation vector $\mathbf{\Omega}$ is horizontal. Assuming that the spinning ball contributes a net circulation to the ambient flow, one expects the air speed to be larger on the upper, retreating surface than on the lower, advancing surface. Bernoulli's Theorem would thus indicate a vertical pressure gradient that will drive the ball upwards, consistent with one's intuition. This physical picture was developed formally by Lord Rayleigh (1877), who solved for inviscid flow around a two-dimensional translating spinning cylinder, the effect of the spin being incorporated by imposing a circulation $\Gamma = \Omega a^2$. His solution indicated that the effect of the circulation was to shift the stagnation points (and associated Bernoulli high pressures) downwards from the leading and trailing edges of the circle, giving rise to an upward lift force per unit length of $\rho U \Omega a^2$ (Figure 6b). In what follows, we shall expose the shortcomings of this inviscid physical picture, demonstrating that the anomalous force may differ from that predicted by Lord Rayleigh not only in terms of magnitude, but direction. In particular, the lift coefficient C_L depends not only on Re, S but is likewise sensitive to the surface roughness in the parameter regime relevant to sports balls in flight.

4.2 The reverse Magnus effect

Having come to grips with the Magnus effect, and the traditional explanation thereof, one can only be puzzled to note that striking a smooth beach ball or an old, worn volleyball with spin has just the opposite effect: the ball bends in the opposite sense relative to a normal football, that is, $C_L < 0$. As we shall see, this arises due to the so-called reverse Magnus effect, a satisfactory explanation of which cannot be given in terms of Bernoulli arguments.

Figure 6a presents data collected from wind tunnel studies indicating the dependence of the Magnus force on both the translational and rotational speeds of a smooth cylinder, specifically, the dependence of the lift coefficent, $C_L = F_M/(\rho a^2 U \Omega)$, on the Reynolds number, $Re = Ua/\nu$, and the spin parameter, $S = \Omega a/U$ (Brown 1971). For $Re < 100,000$, the Magnus force is always positive ($C_L > 0$); however, for $Re > 128,000$, the sign of the Magnus force reverses ($C_L < 0$) over a finite range of rotation rates. This reversal of the direction of the rotation-induced force on a translating sphere is known as the reverse Magnus effect, and is most likely to arise at very large Re. While such a comprehensive data set has not been produced for spheres, the reversal of the sign of C_L at high Re has also been reported (Maccoll 1928, Davies 1949, Barkla *et al.* 1971). The resulting reverse Magnus effect may be rationalized through our discussion in §3 of boundary layers.

Owing to the different local speed difference between the ambient air and points on the

surface of a translating, rotating sphere, the effective Reynolds numbers are different on the advancing and retreating sides of a spinning ball, which may result in two effects. When the boundary layers on both sides are either subcritical or supercritical, reference to Figure 3 indicates that the flow on the advancing side will separate sooner (nearer to the equator) than on the retreating side. The net effect will thus be a deflection of the wake towards the advancing side. For example, for a ball struck with pure backspin, this differential boundary layer separation will result in the wake being deflected downwards, the resulting force on the ball being upwards, as follows from the conservation of momentum (Figure 6c). The resulting force on the spinning ball is thus consistent with that predicted by the inviscid description of the Magnus effect (Figure 6b), but in reality relies critically on a difference in the geometry of boundary layer separation on the advancing and retreating sides of the ball.

We have seen that during the course of a typical shot, the ball decelerates through the drag crisis, its boundary layers transitioning from turbulent to laminar. When the ball is spinning, one expects the drag crisis to be crossed first on the retreating side, where the velocity difference between ball and free stream is minimum. There would thus arise a situation in which the boundary layer is turbulent on the advancing side, and laminar on the retreating side. The resulting delay of boundary layer separation on the advancing side would lead to an asymmetric wake, with air in the wake being deflected in the direction of the retreating side, giving rise to the reverse Magnus effect, and a lift force opposite that expected ($C_L < 0$; Figure 6d). As the ball decelerates further, both boundary layers will transition to laminar, and the lift anticipated on the basis of the traditional Magnus effect ($C_L > 0$) will be restored. To summarize, as a typical shot decelerates through the drag crisis, its Magus force will change sign twice, as the retreating and advancing boundary layers transition in turn from turbulent to laminar.

The critical role of surface roughness on the Magnus effect is illustrated in Figure 7. A smooth plastic ball (similar to a beach ball) is struck with the instep in such a way as to impart typical spin (with the vorticity vector vertical). Its trajectory is marked with blue circles. If it were a regular football, the ball would curve towards the shooter's left in response to the Magnus force; however, because it is smooth, the reverse Magnus effect applies, and the ball curves towards the shooter's right. The red trajectory indicates the trajectory of the same ball struck in precisely the same way; however, this time a single elastic band is wrapped around the ball's diameter. This rubber band is sufficient to ensure turbulent boundary layer separation on both sides of the spinning ball, so that the regular Magnus effect arises. The ball with the rubber band thus responds to rotation as does a regular football, and swerves to the shooter's left.

We thus see the critical role of surface roughening on the flight of the football. It is noteworthy that, since the inception of the sport, footballs have always had significant roughness, first in the form of stitched seams between panels. Moreover, the shape of these panels has changed dramatically (Figure 8). The aerodynamic performance of a number of

recent panel patterns has been investigated by Alam et al. (2011), who demonstrate that, while the balls' aerodynamic performance is sensitive to the presence of panels, it is not greatly altered by their particular form. In modern times, when it is entirely possible to produce a perfectly smooth ball, manufacturers choose not to do so for an obvious reason: the ball would, over a greater range of parameters, bend the wrong way.

5 Brazilian Free Kicks

Just as the Canadian Inuit are alleged to have hundreds of words for snow and ice, the Brazilians have an entire lexicon devoted to different styles of free kicks. We proceed by rationalizing the anomalous motion of each of the different styles in terms of the aerodynamics of balls in flight. The Chute de Curva describes classic bending of the ball, the simplest in terms of execution. For a right footer, one strikes the ball with the instep, sweeping the foot past as one does so, thus imparting a counterclockwise spin as viewed from above, a vertical $\mathbf{\Omega}$. In response, the ball 'bends' to its left as it flies through the air (Figure 6). The change in trajectory can be significant, with the ball moving laterally several meters during flight.

The Trivela (or 'Tres Dedos') is instead struck with the outside of the foot, with one's three outer toes as suggested by its name. This imparts the opposite spin to the ball, which thus (for a right footer) curves in the opposite direction, to the shooter's right. Owing to the decreased contact area during the foot strike, the trivela is generally more difficult to control than the Chute de Curva. The most celebrated trivela is undoubtedly that of Roberto Carlos in 1997 in the Tournoi de France, struck in a friendly against France from a distance of 37 meters (Dupeux *et al.* 2010). Careful viewing indicates that, had the ball followed its initial trajectory, it would have crossed the goal line roughly on the edge of the 18 meter box. However, owing to the spin-induced curvature of its flight, it nipped just inside the post, past an astonished french keeper.

The Folha Seca is struck with nearly pure topspin by brushing over the ball during the strike. As its name suggests, the ball then dips dramatically, falling like a dead leaf. While volleying a ball with topspin is relatively straightforward, imparting pure topspin is extremely difficult to do from a dead ball, and only a few players have truely mastered it. The Brazilian old-timers speak of Didi as its inventor, while Juninho Pernambucano and Cristiano Ronaldo are perhaps its best modern practitioners. The most visually striking shot in football deserves its colorful brazilian name, the Pombo Sem Asa. Struck hard and clean with no spin imparted at impact, the ball rockets through the air, moving erratically up and down, from side to side, like a Dove without Wings. Its unpredictability renders it fearsome for goalkeepers, who find it extremely difficult to judge. Free-kick specialists know that both the Folha Seca and the Pombo Sem Asa are best induced by striking the ball's valve.

While four free kick styles are enumerated above, there are only two physical effects that need to be understood to rationalize them. The Magnus effect allows one to rationalize the lateral curvature of both the Chute de Curva and the Trivela, as well as the anomalous dip of the Folha Seca. The origins of the unpredictable trajectory of the Pombo Sem Asa are not as well understood. We have seen that as a ball passes through the drag crisis, the sign of the lift force is expected to change twice as the retreating and advancing sides of the ball transition in turn from turbulent to laminar. If the shot changes direction more than twice, then an alternate mechanism must be sought. One candidate is the knuckling effect prevalent when baseballs are thrown with very little spin (Mehta and Pallis, 2001). Here, the orientation of the flow in the turbulent wake changes slowly in response to the slowly changing orientation of the seams. As each vortex shed in the wake of the ball represents a pressure anomaly, the changes in the vortex distribution are reflected in a time-varying aerodynamic force on the ball and an unpredictable trajectory. Despite the absence of pronounced seams on a volleyball, a similar knuckling effect arises when the ball is struck with very little spin (Mehta & Pallis, 2001).

6 Discussion

We have presented a rather idiosynchratic review of the dynamics of footballs in flight, highlighting the dominant influence of aerodynamics on their trajectories. We have seen that the interaction of surface roughness and boundary flows is critical in many aspects of football dynamics. Specifically, it prescribes both the aerodynamic drag on the ball, and so the range of goal kicks, as well as the anomalous lateral forces acting on rotating or non-rotating balls in flight. The Magnus effect allows one to rationalize the anomalous curvature of spinning balls, including the extended range of goal kicks struck with backspin, and the bending of free kicks around or over a wall of defenders with the Chute de Cura or Folha Seca, respectively.

We have elucidated the relatively complex physics behind the fact that the aerodynamic drag acting on a football in flight is proportional to $\rho U^2 \pi a^2$, and may be understood as being due to a pressure difference of order ρU^2 between the leading and trailing sides of the ball induced by boundary layer separation. The fact that this drag depends on the air density ρ suggests a dependence of the ballistic performance on the atmospheric conditions. For example, at Mexico City, at an altitude of 2.2km, the air density is roughly 80% that at sea level. Thus, a 25m shot will arrive approximately 0.02 seconds sooner, during which time a goalie lunging at 10m/s will cover a distance of 20cm. One thus sees that playing at altitude gives an advantage to the shooter, and tends to favor high-scoring matches. Of course, this aerodynamic advantage may be more than offset by the cardiovascular penalties associated with playing at altitude.

We have reviewed the standard inviscid treatment of flow past a spinning cylinder, typi-

cally the rationale provided for the Magnus effect, and found it wanting. While it predicts the correct direction for the Magnus force (based on the intuition of the soccer or tennis player), we have seen that this result is purely fortuitous. Specifically, we have seen that the Magnus force on a smooth, light sphere may act in a direction opposite to that on a football, as may be readily observed by kicking a beach ball. The fact that the sign of the Magnus force can reverse on nearly identical spinning balls (Figure 7) highlights the critical role of surface roughness and boundary layers in the Magnus effect. We feel confident in predicting that, however much manufacturing techniques evolve, there will always be roughness elements on the football; otherwise, players will have to adjust to the reverse Magnus effect.

We have reviewed the brazilian lexicon of free kicks, and provided rationale for the behaviour of each. The bulk can be understood simply in terms of the Magnus effect, the exception being the Pombo Sem Asa, which is struck without spin. Two possible rationale for the resulting irregular trajectory have been proposed. The first would indicate that the Pombo Sem Asa is the footballing equivalent of the knuckleball, its unpredictable trajectory due to the random shedding of vortices in its wake. Hong et al. (2010) performed wind-tunnel studies, in which the wake of the ball was visualized by dust placed on its surface. They note that the vortex shedding arises at a much higher frequency than the directional changes of the ball. This would suggest that a more plausible rationale would be the double reversal of the sign of the lift force as the ball decelerates through the drag crisis. The relative importance of random vortex shedding and the drag crisis in the erratic flight of the Dove Without Wings remains a subject of active research.

Another important aspect of the dynamics of football that I have not touched upon is the striking of the ball. The contact time between foot and ball was measured by Nunome et al. (2012), and found to be approximately 10ms; however, this value will in general depend on both the geometry of the foot strike, and the overpressure of the ball. FIFA stipulates that internal overpressures lie in the rather sizable range of 0.6 to 1.1atm. Within this range, contact times vary by approximately 20%, being larger for the softer balls. The contact time will in general determine the ability of the shooter to control the ball. In particular, the longer the contact time, the more readily the shooter can impart spin to the ball when trying to bend it. Conversely, if the shooter wants to strike the ball without spin, and so produce a Pombo Sem Asa, it is advantageous to minimize the contact time. The latter is consistent with the fact that in attempting to generate such a knuckling effect, many free-kick specialists strike the valve side of the ball, where the ball is relatively stiff and uncompliant, so as to minimize contact time.

We can now apply what we have learned to the puzzling question that faced me as a player when, having grown accustomed to playing in Boston's hot, dry summers, I had to adjust to the wet, wintry pitches of England. It became immediately apparent that bending the ball in a controlled fashion was significantly more difficult in the English winter, at times virtually impossible. We can see now why such would be the case. The balls in England

were often water-logged, thus heavier and more slippery, as well as overpumped. As a result, imparting controlled spin was more difficult. Moreover, the additional weight of the wet ball insured that the ball's effective coefficient of ballistic performance was higher, so they would respond less to the Magnus force. I can thus rationalize why my first attempts to bend the ball at the Fitzwilliam College grounds flew scud-like, well wide of both the wall and the net, and why I was subsequently relegated to the role of fair weather free kick specialist.

Acknowledgements: The author thanks Daniel Harris and Lisa Burton for their assistance in the preparation of Figures 1 and 7, Karl Suabadissen for his experiments that culminated in Figure 7. I also thank countless football friends for valuable discussions, and André Nachbin and Christophe Clanet for careful readings of the manuscript.

References

Acheson, D. J., 1990. *Elementary Fluid dynamics*, Oxford University Press, Oxford.

Adair, R.K., 2002. *The physics of baseball* (Harper Collins, New York).

Alam, F. , Chowdhury, H., Moria, H. and Fuss, F.K., 2010. A Comparative Study of Football Aerodynamics, *Procedia Engineering*, **2**, 2443-2448.

Anderson, J.D., 2005. Ludwig Prandtl's boundary layer, *Physics Today*, December **2005**, 42–45.

Anonymous, 1930. Whirling spools lift this plane, *Popular Science Monthly*, November 1930.

Asai, T., Seo. K. Kobayashi, O. and Sakashita, R., 2007. Fundamental aerodynamics of the soccer ball, *Sports Engineering*, **10**, 101–110.

Barkla, H. M. and Auchterloniet, L.J., 1971. The Magnus or Robins effect on rotating spheres, *J. Fluid Mech.*, **47**, 437–447.

Batchelor, G. K., 1967. *An introduction to fluid mechanics*, Cambridge University Press: Cambridge.

Brown, F. N. M., 1971. *See the wind blow*, University of Notre Dame, Indiana.

Daish, C. B., 1972. *The physics of ball games*, (English Universities Press: London).

Davies, J.M., 1949. The aerodynamics of golf balls, *J. Appl. Phys.*, **20**, 821–828.

Dupeux, D., Le Goff, A., Quéré, D and Clanet, C., 2010. The spinning ball spiral, *New J. Physics*, **12**, 093004.

Erlichson, H. , 1983. Maximum projectile range with drag and lift with particular appli-

cation to golf. *Am. J. Physics*, **51**(4), 357–362.

Frolich, C.,1984. Aerodynamic drag crisis and its possible effect on the flight of baseballs. *Am. J. Physics*, **52**(4),325–334.

Gay, T., 2004. *Football physics: the science of the game*, Rodale Inc.: New York.

Gilmore, C. P., 1984. Spin sail harnesses mysterious Magnus effect for ship propulsion, *Popular Science*, November 1984, p.70–72.

Goff, J.E. and Carré, M.J., 2010. Soccer ball lift coefficients via trajectory analysis, *Eur. J. Phys.*, **31**, 775-784.

Goff, J. E., 2010. Power and spin in the beautiful game, *Physics Today*, July issue, p. 62-63.

Goff, J.E. and Carré, M.J., 2012. Investigations into soccer aerodynamics via trajectory analysis and dust experiments, *Procedia Eng.*, **34**, 158-163.

Hong, S., Chung, C., Nakayama, M. and Asai, T., 2010. Unsteady aerodynamic force on a knuckleball in soccer, *Procedia Eng.*, **2**, 2455-2460.

Hong, S. and Asai, T., 2011. Aerodynamics of knuckling effect shot using kick-robot. *Int. J. Appl. Sports Sci.*, **23** (2), 406-420.

Liger-Belair, G., 2004. *Uncorked: The science of champagne*, Princeton University Press, Princeton.

Lugt, H., 1995. *Vortex flow in nature and technology*, Krieger Publishing Company: Malabar, Florida, USA.

Magnus, G., 1853. Uber die Abweichung der Geschosse, und: Uber eine abfallende Erscheinung bei rotirenden Korpern, *Annalen der Physik*, **164**(1), 129.

Maccoll, J. W., 1928. Aerodynamics of a spinning sphere, *J. R. Aeronaut. Soc.*, **32** (213), 777–798.

Mehta, R. D., 1985. Aerodynamics of sports balls, *Ann. Rev. Fluid Mech.*, **17**, 151–189.

Mehta, R. D., Bentley, K., Proudlove, M. and Varty, P., 1983. Factors affecting cricket ball swing, *Nature*, **303**, 787–788.

Mehta, R. D., 2005. An overview of cricket ball swing, *Sports Eng.*, **4**, 181-192.

Mehta, R.D. and Pallis, J. M., 2001. Sports Ball Aerodynamics: Effects of Velocity, Spin and Surface Roughness, in *Materials and Science in Sport*, Ed. S. Froes, p. 185-197.

Mehta, R.D., Alam, F. and Subic, A. 2008. Review of tennis ball aerodynamics. *Sports Technol.*, **1**, 7–16.

Mehta, R.D., 2009. Sports ball aerodynamics, in *Sport Aerodynamics*, Ed. H. Norstrud, Springer: New York.

Nathan, A. M., 2008. The effect of spin on the flight of a baseball, *Am. J. Phys.*, **76**,

119-124.

Newton I., 1672. New theory of light and colours. *Phil. Trans. Roy. Soc. London* **1**, 678688.

Nunome, H., Shinkai, H., and Ikegami, Y., 2012. Ball impact kinematics and dynamics in soccer kicking, Proc. 30th Annual Conference of Biomechanics in Sports, Melbourne Australia.

Prandtl, L., 1904. Uber Flussigkeitsbewegung bei sehr kleiner Reibung, in *Verhandlungen des dritten internationalen Mathematiker-Kongresses* Heidelberg, ed. A. Krazer (Teubner: Leipzig, Germany), p. 484.

Rayleigh, Lord, 1877. On the irregular flight of a tennis ball. *Messenger of Mathematics.* **7**, 14–16.

Robins, B., 1805. *New Principles of Gunnery*, ed. R. Hutton. First printed in 1742.

Sakamoto, H. and Haniu, H., 1995. The formation mechanics and shedding frequency of vortices from a sphere in uniform shear flow, *J. Fluid Mech.*, **287**, 151–171.

Schlichting, H., 1955. *Boundary-Layer Theory* (New York: McGraw-Hill).

Shapiro, A. H., 1961. Shape and flow: The fluid dynamics of drag (Anchor Books: Boston).

Smith, M.R., Hilton, D.K. and Van Sciver, S.W., 1999. Observed drag crisis on a sphere in flowing He I and He II, *Phys. Fluids*, **11**, 751–753.

Vogel, S., 2003. *Comparative biomechanics: Life's Physical World*, (Princeton University Press: Princeton).

Watts, R.G. and Sawyer, E., 1975. Aerodynamics of a knuckleball. *Am. J. Physics* , **43**(11), 960–963.

Wauthy, G., Leponce, M., Banai, N., Sylin, G. and Lions, J.-C., 1998. The backwards jump of the box mite, *Proc R. Soc. Lond. B*, **265**, 2235–2242.

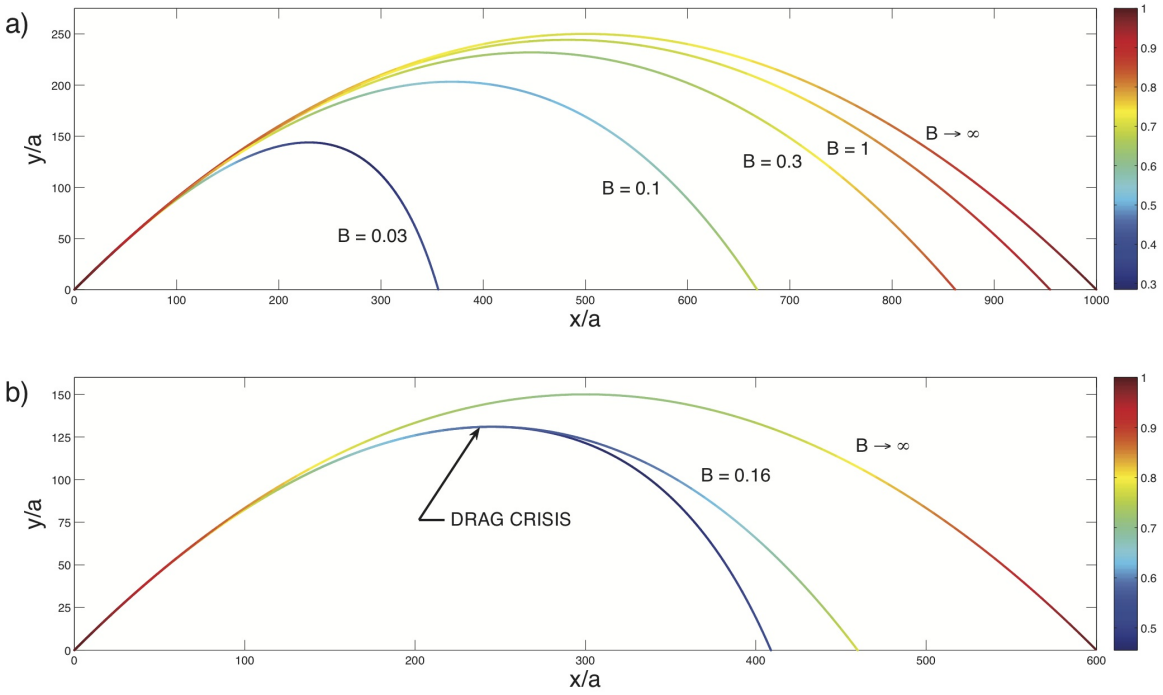

Figure 1: Computed trajectories of non-spinning balls. a) Trajectories of football-sized balls launched at an angle of 45° and an initial speed of 32 m/s (corresponding to $A = 910$; see Figure 2) with different coefficients of ballistic performance. The instantaneous flight speed is prescribed by the color of the curve, and the coordinates scaled by the ball size a. In the limit of $B \to \infty$, aerodynamic effects are negligible: the range is a maximum, and the flight path symmetric about its mid point. As B is decreased progressively, the range is decreased in response to aerodynamic drag, and the symmetry of the trajectory is broken: the ball falls more slowly and more steeply than it rises. b) Computed trajectories of footballs in a vacuum (upper curves) and in standard atmospheric conditions. Balls are launched with initial velocity of 25 m/s (corresponding to $A = 550, B = 0.16$) and take-off angle of 45°. The lower curve indicates the influence of the drag crisis: at $Re = 10^5$, the ball decelerates through the drag crisis, and the drag coefficient C_D increases from 0.1 to 0.4. The resulting increase in drag is reflected in the decreased range and heightened asymmetry of the trajectory. Image courtesy of Dan Harris.

Sport	m (g)	a (cm)	U_0 (m/s)	Re	A	B	S
Shot put	7260	6	10	40,000	170	54	0.05
Basketball	630	11.9	15	120,000	190	0.5	0.07
Tennis	58	3.8	70	180,000	12,000	0.22	0.19
Cricket	160	3.6	40	100,000	4,400	0.2	0.18
Baseball	150	3.66	40	100,000	4,200	0.2	0.05
Football	430	11.3	32	240,000	910	0.1	0.21
Golf	45	2.1	80	110,000	30,500	0.05	0.09
Volleyball	270	10.5	30	210,000	860	0.08	0.21
Squash	24	2.0	70	100,000	24,500	0.03	0.1
Ping-pong	2.5	2	45	60,000	10,125	0.008	0.36

Figure 2: The physical parameters of many common ball sports: a and m correspond to the ball's radius and mass, respectively, U_0 to its peak speed, Ω its spin angular velocity, and $\nu = 0.15$ cm^2/s to the kinematic viscosity of air. The corresponding dimensionless groups: the Reynolds number, $Re = U_0 a/\nu$, the range parameter $A = U_0^2/(ga)$, the coefficient of ballistic performance, $B = mg/(\pi a^2 \rho U_0^2)$ and the spin parameter $S = \Omega a/U_0$. The range parameter A indicates the relative magnitudes of the ball's maximum range in vacuo and its radius. The lower B, the greater the influence of aerodynamic effects on the flight of the ball. The small values of B for most ball sports indicate that the aerodynamic drag exerted at peak speed is typically comparable to or greater than the weight of the ball.

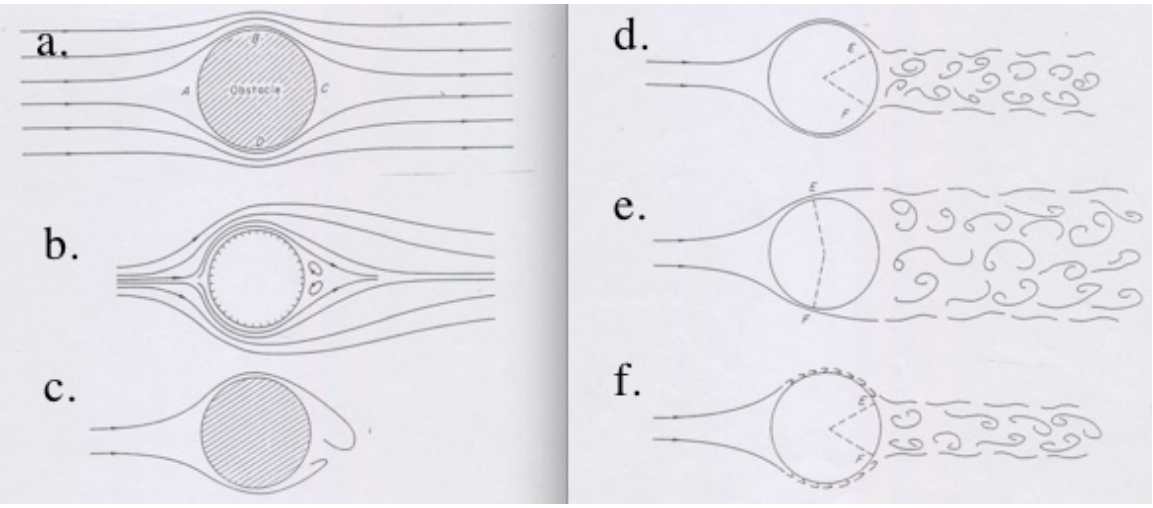

Figure 3: Schematic illustration of the evolution of the flow past a smooth sphere with increasing Reynolds number, $Re = Ua/\nu$. a) For $Re \ll 1$, the streamlines are fore-aft symmetric and the drag is principally of viscous origins. b) For $Re > 10$, boundary layer separation downstream of the sphere induces a vortical wake and a significant pressure drag. c) for $100 < Re < 1000$, the vortical wake becomes unstable, resulting in lateral forces on the sphere. d) for $Re > 1000$, the wake becomes turbulent, its extent being maximum for e) $Re \to 2 \times 10^5$. f) For $Re > 2 \times 10^5$, the boundary layers become turbulent, delaying the boundary layer separation and decreasing the extent of the turbulent wake. Owing to the resulting dramatic reduction in drag on the sphere, the latter transition is called the drag crisis. Note that the precise Re-values at which flow transitions occurs depends strongly on the sphere's surface roughness. Images from Daish (1972).

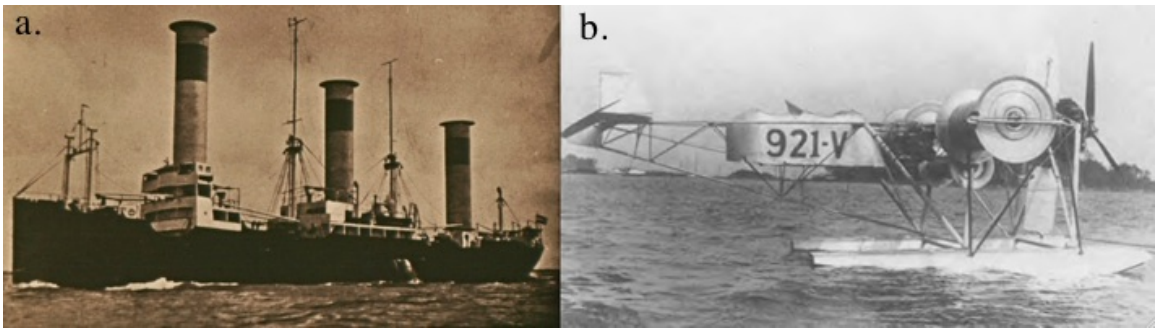

Figure 4: Two applications of the Magnus effect. a) The sail boat *Barbara*, conceived and built by Flettner in the 1920s, has sails with the form of spinning cylinders (Gilmore 1984). b) The rotorplane 921-V, whose wings take the form of spinning cylinders, was developed shortly thereafter (Anon. 1930). Magnus boats were more successful than their airborne counterparts; the former having circumnavigated the globe, the latter having only flown once before crash landing.

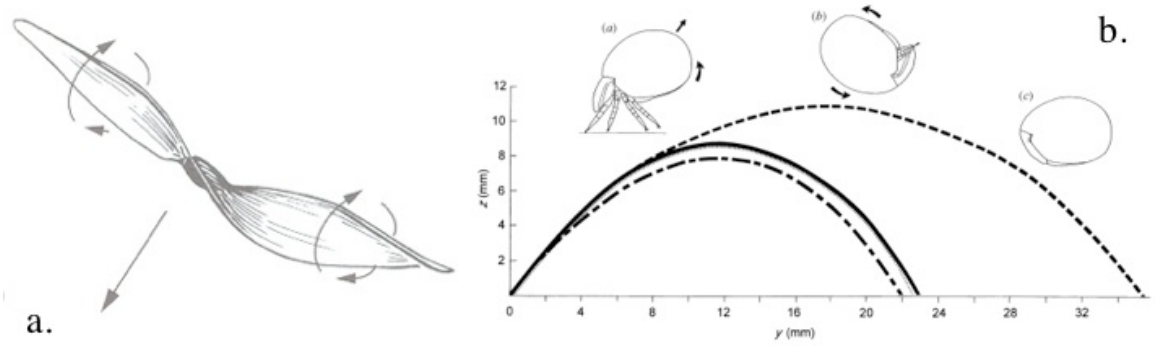

Figure 5: Two examples of the Magnus effect in the natural world. a) Many seed pods are shaped so as to tumble with backspin as they fall, thus extending their range via Magnus lift (Image from Vogel 2003). b) The box mite leaps with backspin, thus extending its range (Image from Wauthy et al. 1998).

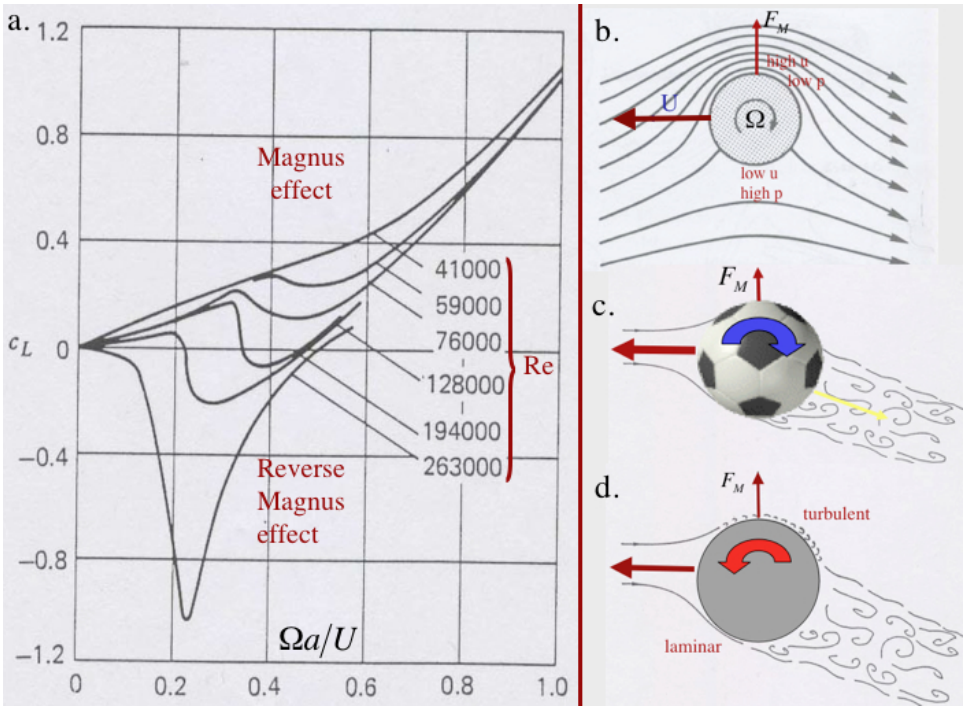

Figure 6: a) The dependence of the Magnus lift coefficient, c_L, on the translational and rotational speeds of a smooth cylinder. The Magnus force per unit length, $F_M = c_L \rho a^2 U \Omega$, where a is the cylinder radius, U its translational speed and Ω its rotational speed. At sufficiently high $Re = Ua/\nu$, we see that $c_L < 0$, indicating a reversal in the sign of the Magnus force. Image from Brown (1971), reprinted from Lugt (1995). b) The idealized picture of inviscid flow past a spinning cylinder, in which a circulation Ωa^2 is imposed on the streaming flow past the body. On the basis of this physical picture, Lord Rayleigh predicted $c_L = 1$. In reality, we see in a) a strong dependence of C_L on both Re and $S = \Omega a/U$, as is the case for spheres. c) For flow past a real football, the spin serves to deflect the flow in the wake downwards, giving rise to a net lift force on the ball. d) The reverse Magnus effect. On a smooth ball, the Magnus force may reverse sign, causing the ball to bend the wrong way. This results from the difference in the boundary layers on the advancing and retreating sides, the former being turbulent, the latter laminar.

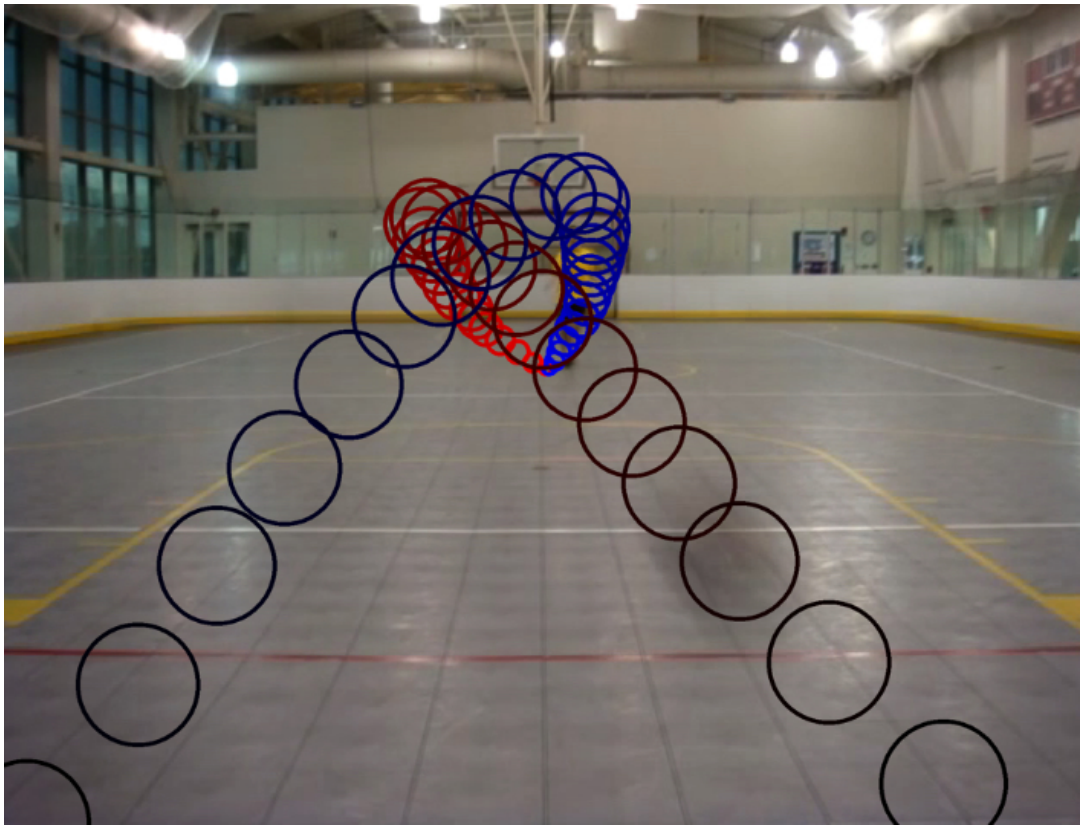

Figure 7: The trajectories of two nearly identically struck balls, one smooth, the other rough, the former responding to the reverse Magnus effect, the latter, the Magnus effect. The ball consists of a smooth beach ball. When struck with the right instep so as to impart rotation in the usual sense, it bends anomalously, from the shooter's left to right ($C_L < 0$; blue trajectory). Adding an elastic band around its equator is sufficient to render the boundary layer turbulent, therefore restoring the expected curvature, from the shooter's right to left ($C_L > 0$; red trajectory). Thanks to Karl Suabedissen for his sniper-like precision, and Lisa Burton for her skillful ball tracking.

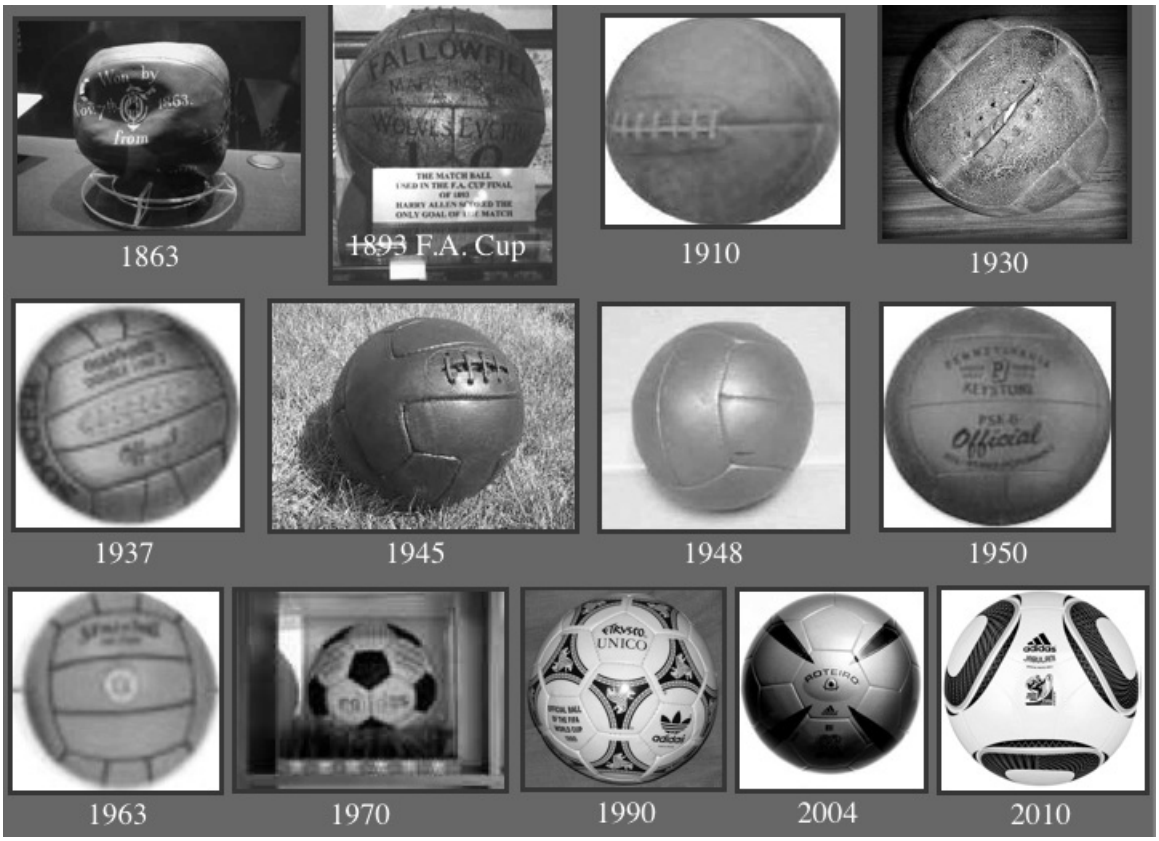

Figure 8: The evolution of the football. While the form of the ball's paneling has changed significantly, surface texture remains a part of the modern ball. While modern fabrication techniques could create a smooth ball, the surface roughness is necessary to ensure that the ball maintains its aerodynamic properties, including its response to induced spin. Images compiled from various on-line sources.